TENTH AUSTRALASIAN FLUID MECHANICS
CONFERENCE - UNIVERSITY OF MELBOURNE
11-15 DECEMBER 1989

PREDICTION OF TURBULENT SWIRLING FLOW IN A DIFFUSER WITH A TAILPIPE

Nam-Hyo CHO and Clive A.J. FLETCHER

Department of Mechanical Engineering
University of Sydney, NSW 2006
AUSTRALIA

ABSTRACT

The turbulent swirling flow in a diffuser with a tailpipe is predicted using a $k-\epsilon$, an algebraic Reynolds stress (ASM) and an ASM turbulence model with a false production term. Inlet swirl profiles of both Rankine- and forced-vortex forms are considered. The inclusion of the false production term in the ASM model is found to be necessary to predict the sustained dip in the axial velocity component with the Rankine-vortex swirl configuration. For the forced-vortex swirl configuration all the turbulence models give similar mean flow predictions.

INTRODUCTION

The achievement of satisfactory pressure recovery in medium angle diffusers, less than 20° total angle, has been investigated widely. But the detailed turbulence flow characteristics through experiments or predictions have not been analyzed sufficiently to understand the crucial flow features. This may be due to the complexity of the flow behaviour.

It is well known that introducing an optimum swirl level, whether of a Rankine-vortex (smaller inner part of solid-body rotational type and outer part of free-vortex type) or a forced-vortex (solid-body rotation) form, may improve the overall pressure recovery (McDonald *et al.* (1971), Okhio *et al.* (1983), Senoo *et al.* (1978)). Fitting a tailpipe to the outlet plane of a conical diffuser may also improve the performance. Flow at the outlet plane of the diffuser may be somewhat non-uniform or asymmetric once the diffuser angle or swirl level is increased to a certain level. The tailpipe makes the flow more uniform so that the pressure recovery may continue to occur further downstream in the tailpipe provided the dissipation of mechanical energy is much less than the flux of mean kinetic energy (Ward-Smith,1980). This class of flow is analyzed using alternative turbulence models in this paper.

Previously, the mixing-length model, the $k-\epsilon$ and the ASM turbulence models have been used to predict the confined swirling flow behaviour in medium angle diffusers with or without a tailpipe (Armfield *et al.* (1989), Hah (1983), Okhio *et al.* (1986)). Most of the earlier predictions were performed using regular grids. The present study adopts a non-orthogonal grid with a non-staggered arrangement of all dependent variables. The Okhio *et al.* (1983) flow case (Fig. 1) was chosen for the study. They used a radial intake type swirl generator. Therefore the axial velocity profile may have a very big dip or reversed flow in the centre-line part of the inlet region depending on the inlet swirl level. The swirl profile shows a Rankine-vortex type behaviour and decreases rapidly to a flat profile downstream. An assumed forced-vortex inlet swirl and a uniform axial velocity are used to compare the flow characteristics and to indicate the pressure recovery performance.

GOVERNING EQUATIONS

The governing equations for steady, incompressible flow may be written in tensor form as follows.

Continuity:

$$U^i{}_{,i} = 0, \tag{1}$$

Momentum (U^i):

$$U^j U^i{}_{,j} + (\overline{u^i u^j})_{,j} = -g^{ij} P_{,j}/\rho + \nu g^{lj} U^i{}_{,lj}, \tag{2}$$

Turbulent kinetic energy (k):

$$U^i k_{,i} = \left((\nu + C_s(k/\epsilon)\overline{u^i u^j})k_{,i}\right)_{,j} + P_k - \epsilon, \tag{3}$$

Dissipation rate of k (ϵ):

$$U^i \epsilon_{,i} = \left((\nu + C_\epsilon(k/\epsilon)\overline{u^i u^j})\epsilon_{,i}\right)_{,j} + C_{\epsilon 1}(\epsilon/k)P_k - C_{\epsilon 2}\epsilon^2/k, \tag{4}$$

where U^i is the mean velocity; u^i the fluctuating velocity, g^{ij} the metric tensor, P the pressure, ν the kinematic viscosity, ρ the density, $\overline{u^i u^j}$ the Reynolds stress tensor and $P_k (\equiv -\overline{u^i u^j} U_{i,j})$ the production rate of k. Superscripts indicate contravariant quantities, subscripts indicate covariant quantities, apostrophes in the lower position indicate covariant derivatives.

$k-\epsilon$ turbulence model

To calculate the Reynolds stress tensor appearing in the above equations, the $k-\epsilon$ and algebraic Reynolds stress turbulence models are used. For the $k-\epsilon$ turbulence model Boussinesq's eddy-viscosity concept is written as,

$$\overline{u^i u^j} = -\nu_t (g^{jl} U^i{}_{,l} + g^{il} U^j{}_{,l}) + 2/3 g^{ij} k, \tag{5}$$

where ν_t is the turbulent eddy viscosity defined as $\nu_t \equiv C_\mu k^2/\epsilon$. Then an effective viscosity ν_{eff} is defined by $\nu + \nu_t$. The diffusion terms in the above k and ϵ equations are modeled as $g^{ij}\left((\nu_{eff}/\sigma_k)k_{,i}\right)_{,j}$ and $g^{ij}\left((\nu_{eff}/\sigma_\epsilon)\epsilon_{,i}\right)_{,j}$ respectively.

Algebraic Reynolds stress turbulence models

For the algebraic Reynolds stress turbulence models we used Rodi's approximation (Rodi,1976). Rodi assumed that the net transport of Reynolds stress is proportional to the net transport of k with a multiplication factor $(\overline{u^i u^j}/k)$. The final algebraic form can be written as,

$$(\overline{u^i u^j}/k)(P_k - \epsilon) = P^{ij} + \Phi^{ij} - 2/3 g^{ij}\epsilon - \psi A^{ij}, \tag{6}$$

where,

$$P^{ij} = -\overline{u^i u^m} U^j_{,m} - \overline{u^j u^m} U^i_{,m},$$
$$\Phi^{ij} = \phi_1^{ij} + \phi_2^{ij} + \phi_{w1}^{ij} + \phi_{w2}^{ij},$$
$$\phi_1^{ij} = -C_1 \frac{\epsilon}{k}(\overline{u^i u^j} - 2/3 g^{ij} k),$$
$$\phi_2^{ij} = -C_2(P^{ij} - 2/3 g^{ij} P_k),$$
$$\phi_{w1}^{ij} = C_1' \frac{\epsilon}{k}(\overline{u^n u^n} g^{ij} - 3/2 \overline{u^n u^i} g^{nj} - 3/2 \overline{u^n u^j} g^{ni}) f,$$

$$\phi_{w2}^{ij} = C_2'(\phi_2^{nn} g^{ij} - 3/2\phi_2^{ni} g^{nj} - 3/2\phi_2^{nj} g^{ni}) f,$$

$$A^{ij} = U^k(h_i h_j \frac{\partial(1/h_i h_j)}{\partial x^k} \overline{u^i u^j} + \Gamma^i_{mk} \overline{u^m u^j} + \Gamma^j_{mk} \overline{u^m u^i}).$$

P^{ij} is the production rate of $\overline{u^i u^j}$; Φ^{ij} the pressure-strain term. ϕ_1^{ij} and ϕ_2^{ij} were modeled by Rotta (1951) and Naot *et al.* (1970) respectively. So-called 'wall-echo' terms, ϕ_{w1}^{ij} and ϕ_{w2}^{ij}, account for the increased anisotropy due to the pressure reflection at the wall and were modeled by Shir (1973) and Gibson and Launder (1978). $f(= C_\mu^{3/4} k^{3/2}/(\kappa x_n \epsilon))$ is a wall damping coefficient to account for the wall reflection effect of pressure-strain terms in the near wall region. κ is the Von Karman constant. n denotes the normal direction to the wall. For the present analysis simply the normal distance from a point of interest to the wall is used for x_n. For the references appearing in this section see Sloan *et al.* (1986).

A^{ij} is a so-called 'added' convection term (Sloan *et al.*, 1986) or 'false' production (FP) term (Armfield, 1987). 'Additional' non-gradient convective stress terms arise when the cylindrical or spherical polar coordinates are used for the derivation of Rodi's approximation. These terms may be large relative to the gradient convective stress terms in a highly strained swirling flow. ψ is an arbitrary constant between zero and one. h_i is $g_{ii}^{1/2}$ and Γ^i_{jk} is a Christoffel symbol. Eq. (6) may be further expanded to form a 6×6 matrix system for $\overline{u^i u^j}$ that can be easily inverted. The constants used in the models are given standard values commonly used; $C_\mu = 0.09$, $\sigma_k = 1.0$, $\sigma_\epsilon = 1.22$, $C_{\epsilon 1} = 1.44$, $C_{\epsilon 2} = 1.92$, $C_1 = 1.8$, $C_2 = 0.6$, $C_1' = 0.5$, $C_2' = 0.3$, $C_s = 0.22$, $C_\epsilon = 0.15$.

NUMERICAL SCHEMES

Transformed equations

The governing equations are first converted to the Cartesian or cylindrical coordinate ones and to the generalized coordinates using a transformation rule. The Cartesian or cylindrical velocity components and Reynolds stresses are used for the dependent variables, directly. The final transformed equations are shown in Cho and Fletcher (1989). The transformed equations are integrated on finite volume cells to get a linearized system of equations which is solved by the SIMPLEC (Van Doormaal and Raithby,1984) interative algorithm for fully elliptic equations. The momentum interpolation method of Rhie and Chow (1983) is used to prevent chequer-board oscillations in the pressure field which are common for locally non-staggered velocity-pressure methods. To minimize possible numerical diffusion caused by coarse grids the QUICK (Leonard,1979) scheme is used. Detail descriptions of the transformation, geometrical analysis and solution algorithms may be found in Burns and Wilkes (1987).

A multi-surface grid generation method due to Eiseman (1979) is used for the present two dimensional geometry as shown in Fig. 1. It is possible to generate a near-orthogonal grid at the domain boundaries where the near-orthogonality is assumed for some calculations.

Boundary conditions

The two-layer wall function of Chieng and Launder (1980) is applied for the governing equations of the velocity components and k at the first grid points away from the wall. ϵ is calculated by a simple algebraic form based on the local-equilibrium condition. At the axis the normal gradient of all variables is set to zero, but the velocity component normal to the axis is set to zero. At the exit the normal gradient of all variables is set to zero, but the mass flow constraint is applied for the velocity at every iteration. At the inlet axial (U), radial (V), swirl or circumferential (W) velocities, k and ϵ, if experimental data is available, are specified. For Okhio *et al.* (1983) flow only U and W are available, so V is estimated from the continuity equation. k is set to 0.5% of $(U^2 + W^2)$. ϵ is obtained from $C_\mu^{3/4} k^{3/2}/L$; L is set to 0.01. The normal gradient of all the other variables is set to constant on the inlet plane.

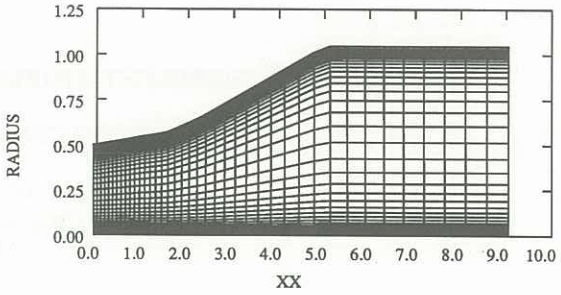

Fig. 1: Computational grid (radius scale ×4.4)

It is considered that the numerical diffusion is not a serious problem as QUICK scheme is used throughout in this study. Three different grid systems (25×25, 40×40,60×60) were used to test the grid independence. Overall solutions are not very different so that the 40×40 grid is used for all the other calculations. A stretched grid is used in both directions and a very fine grid is used in the near axis and wall regions. But the first grid points are set to have $y^+(\equiv y\sqrt{\tau_w/\rho}/\mu) = 50 \sim 130$, where y is the perpendicular distance from the wall to the point; τ_w the wall shear stress, μ viscosity. The solution is taken as converged when the total mass flow residual divided by the inlet mass flow rate is less than 5×10^{-5}.

RESULTS AND DISCUSSION

Rankine-vortex inlet swirl

Predictions of mean flow are presented in this section corresponding to the experimental data of Okhio *et al.* (1983). The experimental data consists of the radial distributions of U and W at the axial locations shown in Figs. 2 and 3. Reynolds number based on the diameter of inlet section ($2R$) is 5.2×10^5 and the swirl number $SN = 0.055$, where

$$SN = \int_0^R UWr^2 dr/(R\int_0^R U^2 r dr). \qquad (7)$$

The diffuser section is not exactly conical in shape but has an initial 5.22° total angle section ($xx = 0.0 \sim 1.55$), a final 16.5° total angle section ($xx = 2.32 \sim 5.00$) and a transition section in between. The tailpipe length is $8R$. All the values appearing in this paper are non-dimensionalized by the inlet diameter ($0.122m$) and the inlet mean axial velocity ($72.44m/s$).

Fig. 2 shows the radial distribution of axial velocity on the normal line to the axis at the station xx. With a stronger swirl the actual experiment shows a flow reversal even at the inlet plane ($xx = 0.0$). The corresponding inlet swirl profile represents a Rankine-vortex form as shown in Fig. 3. These inlet profiles are typical distribution for this type of swirl generator and Senoo *et al.* (1978) also show very similar behaviour. At $xx = 1.55$ in the 5.22° diffuser part all the turbulence models predict the axial velocity correctly in the core region but do not produce such a big dip in the axial velocity except the ASM+FP turbulence model. For the ASM+FP turbulence model $\psi = 0.4$ in Eq. (6) is used. Computation shows a small recirculation bubble in this area when a higher ψ value is used. Okhio *et al.* (1986) with a mixing length model predict a similar result to the present $k - \epsilon$ turbulence model.

At $xx = 5.72$, which is right after the diffuser oulet plane, the experimental velocity profile shows an asymmetry, therefore average values are taken with the correct mass flow. Flow visualization shows a near-wall flow separation between $xx = 3.5 \sim 5.7$ which is not clear in the quantitative experimental data. The ASM and ASM+FP turbulence models show nearly the same result. The ASM turbulence models seem to overpredict in the centre-line region. The ASM turbulence models predict a small separation bubble near the wall at $xx = 3.9 \sim 5.1$, but the $k-\epsilon$ turbulence model does not. An interesting fact is that the ASM+FP turbulence model seems to predict more accurately than the others turbulence models when the axial

velocity profile sustains a dip near the axis. We assume that the full Reynolds stress model may be useful for such a case. But we found that the correct initial profiles are also very important for a good prediction. A roughly estimated radial velocity (V) from the continuity equation gives a lot better prediction all over the domain than if it is simply set to zero. An optimum ϵ level is chosen after a few trial runs. It is hard to say whether the turbulence models used here are good enough to predict mean velocity because of the crucial role of initial profiles.

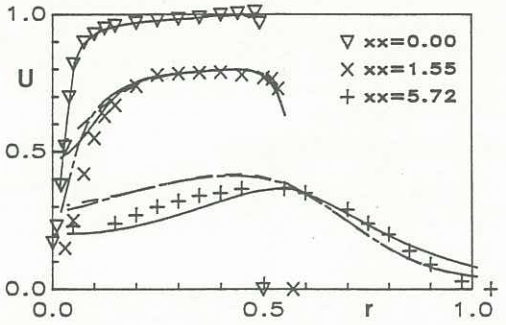

Fig. 2: Axial velocity for the Rankine-vortex inlet swirl (solid line; $k-\epsilon$, dashed; ASM, solid-dashed; ASM+FP). Same notation in the following figures.

Fig. 3 shows the swirl velocity profiles. In the diffuser section the peak swirl level decreases rapidly and the swirl shows a very flat distribution in the tailpipe section. The $k-\epsilon$ turbulence model is slightly more accurate than the other turbulence models at $xx = 1.55$, but all the turbulence models underpredict the peak swirl level. At $xx = 3.48$ all the turbulence models predict the overall level reasonably. The ASM+FP turbulence model seems to overpredict slightly in the core region.

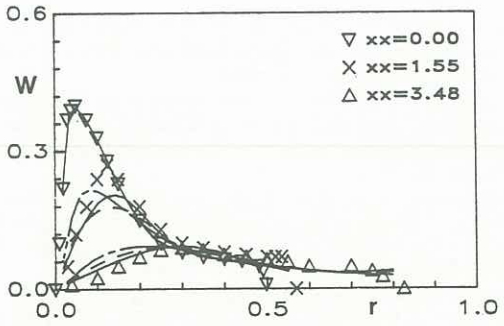

Fig. 3: Swirl velocity

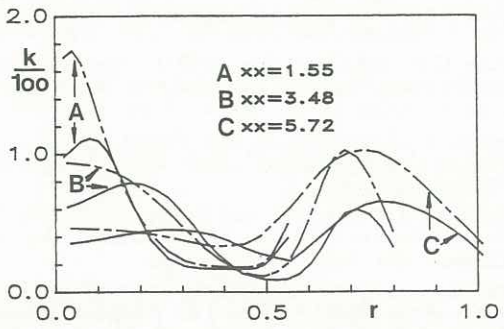

Fig. 4: Turbulent kinetic energy

Fig. 4 shows the turbulent kinetic energy distribution. No experimental data is available for comparison. In the centre-line part of the inlet region the ASM+FP turbulence model shows a much higher level of k than the ASM (not shown) and $k-\epsilon$ turbulence models. From Fig. 2, it appears that the k level may be driven by $\partial U/\partial r$ for this region. At $xx = 5.72$ the ASM turbulence models predict that the near-wall peak level is much higher than predicted by the $k-\epsilon$ turbulence model. This higher level may be associated with the predicted separating flow in the corner region of the diffuser outlet plane. The ASM turbulence model (not shown) shows nearly same distribution as the ASM+FP turbulence model in the near-wall region.

Forced-vortex inlet swirl

To investigate the effect of inlet swirl velocity distribution on the general flow behaviour we assume a uniform axial velocity and a forced-vortex swirl profile at the inlet plane. No experimental data is available for the same geometry of Okhio *et al.* (1983). A uniform U at the inlet is set to 1.0 with a very thin boundary layer thickness. The peak value of W is set to 0.6 very near the wall which gives a swirl number 0.3. The core region turbulence intensity is assumed to be about 3%. L to calculate ϵ is set to 0.01.

Fig. 5 shows the axial velocity distribution. A uniform distribution is predicted in the inlet region. Downstream the near-wall axial velocity is increased at a greater rate than the non-swirl case (not shown) and the profile at the centre-line shows a dip influenced by the mass flow constraint. The $k-\epsilon$ turbulence model predicts a big recirculating bubble around $xx = 4.1 \sim 6.3$. All the turbulence models produce nearly the same result in the diffuser section but the near-wall velocity level of the $k-\epsilon$ turbulence model is a slightly higher than that for the ASM turbulence models in the tailpipe section. It is very hard to find any difference in Figs. 5 to 7 between the two ASM turbulence models which show very different predictions in the centre-line part of the diffuser for a Rankine-vortex inlet swirl (Figs. 2 to 4). This may suggest that the ASM+FP turbulence model is more effective than the ASM turbulence model in that particular flow case.

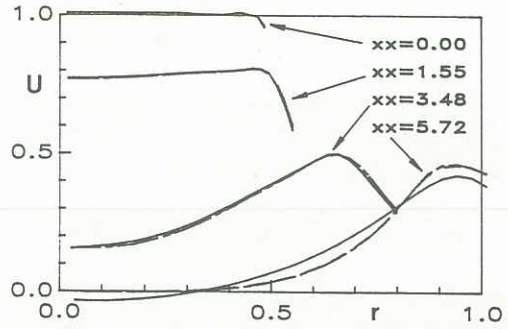

Fig. 5: Axial velocity for the forced-vortex inlet swirl

Fig. 6 shows the swirl velocity profile. The profile maintains a forced-vortex swirl form in the 5.22° angle diffuser section and the near-wall swirl level is decreasing downstream. The ASM turbulence model predictions are very similar all over the region. At $xx = 5.72$ the $k-\epsilon$ turbulence model predicts a higher angular momentum than the ASM turbulence models. It is interesting to note that the boundary layer of W is not developing so much as that of U downstream. The U and W velocity distributions (Figs. 5 and 6) are similar to the case of Armfield *et al.* (1989) who have analyzed a forced-vortex inlet swirl flow, with the same swirl number, in a 20° conical diffuser without a tailpipe.

Fig. 7 shows the turbulent kinetic energy distribution. The distribution at the first two stations follows a typical variation as shown in Armfield *et al.* (1989). The near-wall k peak is increased in the corner region of the diffuser inlet plane and decreases subsequently downstream while the low k level in the core region is maintained. The levels of k and the Reynolds shear stresses (not shown) downstream of $xx = 3.48$ are increased significantly. This may be caused

by a recirculation bubble on the axis near the diffuser exit plane. Depending on the diffuser angle value or the inlet swirl strength, the size of a recirculation bubble changes and the level of turbulence quantities as well. The $k-\epsilon$ turbulence model predicts the overall level to be much higher than that of the ASM turbulence models at $xx = 5.72$ in tailpipe section. A comparison of Figs. 6 and 7 with Figs. 3 and 4 indicates that a forced-vortex inlet swirl flow is effective in suppressing turbulence in the core region, i.e. stabilizing the flow, upstream of the recirculation.

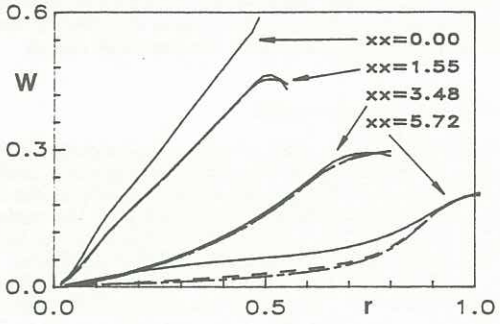

Fig. 6: Swirl velocity

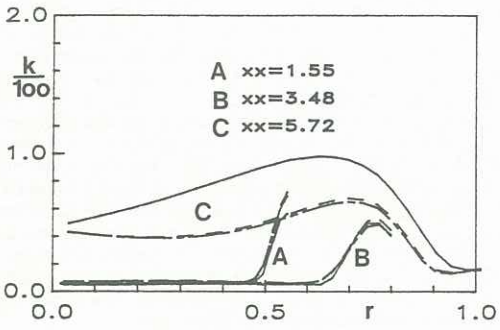

Fig. 7: Turbulent kinetic energy

Fig. 8 shows the pressure recovery performance (C_{PRS}) of the forced-vortex inlet swirl flows when using the $k-\epsilon$ turbulence model. C_{PRS} is a diffuser performance coefficient defined by the area average as,

$$C_{PRS} = \frac{(1/A_2)\int P_2 dA_2 - (1/A_1)\int P_1 dA_1}{1/2\rho(1/A_1)\int U_1^2 dA_1}, \qquad (8)$$

where the subscripts 1 and 2 denote the inlet ($xx = 0.0$) and the outlet ($xx = 5.0$) plane of diffuser respectively. A is the cross sectional area and U_1 is the vector sum of velocity components at the inlet plane. The differences in C_{PRS} from the other turbulence models and the hybrid convective scheme are no more than 2%. Even if the experimental data is not available the prediction indicates the maximum pressure recovery may be obtained around $SN = 0.2 \sim 0.3$.

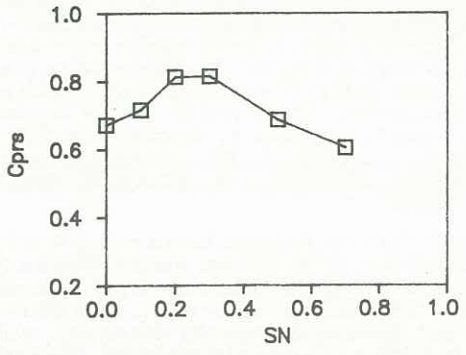

Fig. 8: Pressure recovery

CONCLUSIONS

A Rankine-vortex inlet swirl flow and a forced-vortex inlet swirl flow in a medium angle diffuser with a tailpipe are predicted using a $k-\epsilon$ and algebraic Reynolds stress models with/without a false production term. The algebraic Reynolds stress model with a false production term is more effective in representing the sustained downstream dip in the axial velocity component near the diffuser entrance when the inlet flow is of a Rankine-vortex type. However further downstream all the turbulence models produce qualitatively similar distributions. For a forced-vortex inlet swirl flow all the turbulence models produce similar mean flow and k distributions except that the $k-\epsilon$ turbulence model indicates a higher k level in the tailpipe region. There is an optimum swirl level ($SN = 0.25$) to get the maximum pressure recovery for a forced-vortex inlet swirl flow in this geometry.

ACKNOWLEDGEMENT

The authors are grateful to the Australian Research Council (ARC) for their continuing support.

REFERENCES

Armfield, S.W. (1987), "Numerical Simulation of Incompressible Turbulent Swirling Flow in Conical Diffusers", Ph.D. Thesis, University of Sydney, Australia.

Armfield, S.W., Cho, N.-H. and Fletcher, C.A.J. (1989), "Prediction of Turbulence Quantities for Swirling Flow in Conical Diffusers", *AIAA J.*, to appear.

Burns, A.D. and Wilkes, N.S. (1987), "A Finite Difference Method for the Computation of Fluid Flows in Complex Three Dimensional Geometries", Harwell Laboratory, Oxford, AERE R 12342.

Chieng, C.C. and Launder, B.E. (1980), "On the Calculation of Turbulent Heat Transport Downstream from an Abrupt Pipe Expansion", *Num. Heat Transfer*, pp. 189-207.

Cho, N.-H. and Fletcher, C.A.J. (1989), "Prediction of Turbulent Swirling Diffuser Entrance Flows", Int. Symp. on Comp. Fluid Dyn.-Nagoya, Japan, August 28-31.

Eiseman, P.R. (1979), "A Multi-Surface Method of Coordinate Generation", *J. of Comp. Phys.*, Vol. 33, pp. 118-150.

Hah, C. (1983), "Calculation of Various Diffuser Flows with Inlet Swirl and Inlet Distortion Effect", *AIAA J.*, Vol. 21, No. 8, pp. 1127-1133.

Leonard, B.P. (1979), "A Stable and Accurate Convective Modelling Procedure Based on Quadratic Upstream Interpolation", *Comp. Meth. in Applied Mech. and Eng.*, Vol. 19, pp. 59-98.

McDonald, A.T., Fox, R.W., and Van Dewoestine, R.V. (1971), "Effects of Swirling Inlet Flow on Pressure Recovery in Conical Diffusers", *AIAA J.*, Vol. 9, No. 10, pp. 2014-2018.

Okhio, C.B., Horton, H.P. and Langer, G. (1983), "Effect of Swirl on Flow Separation and Performance of Wide Angle Diffusers", *Int. J. Heat and Fluid Flow*, Vol. 4, No. 4, pp. 199-206.

Okhio, C.B., Horton, H.P. and Langer, G. (1986), "The Calculation of Turbulent Swirling Flow through Wide Angle Conical Diffusers and the Associated Dissipative Losses", *Int. J. Heat and Fluid Flow*, Vol. 7, No. 1, pp. 37-48.

Rhie, C.M. and Chow, W.L. (1983), "Numerical Study of the Turbulent Flow Past an Airfoil with Trailing Edge Separation", *AIAA J.*, Vol. 21, No. 11, pp. 1525-1532.

Senoo, Y., Kawaguchi, N., and Nagata, T. (1978), "Swirl Flow in Conical Diffusers", *Bull. J.S.M.E.*, Vol. 21, No. 151, pp. 112-119.

Sloan, D.G., Smith, P.J. and Smoot, L.D. (1986), "Modeling of Swirl in Turbulent Flow Systems", *Prog. Energy Combust. Sci.*, Vol. 12, pp. 163-250.

Van Doormaal, J.P. and Raithby, G.D. (1984), "Enhancements of the SIMPLE Method for Predicting Incompressible Fluid Flow", *Num. Heat Transfer*, Vol. 7, pp. 147-163.

Ward-Smith, A.J. (1980), Internal Fluid Flow, Clarendon Press, Oxford.